

Lifting-wing Quadcopter Modeling and Unified Control

Quan Quan*, Shuai Wang, and Wenhan Gao

Hybrid unmanned aerial vehicles (UAVs) integrate the efficient forward flight of fixed-wing and vertical takeoff and landing (VTOL) capabilities of multicopter UAVs. This paper presents the modeling, control and simulation of a new type of hybrid micro-small UAVs, coined as lifting-wing quadcopters. The airframe orientation of the lifting wing needs to tilt a specific angle often within 45 degrees, neither nearly 90 nor approximately 0 degrees. Compared with some convertiplane and tail-sitter UAVs, the lifting-wing quadcopter has a highly reliable structure, robust wind resistance, low cruise speed and reliable transition flight, making it potential to work fully-autonomous outdoor or some confined airspace indoor. In the modeling part, forces and moments generated by both lifting wing and rotors are considered. Based on the established model, a unified controller for the full flight phase is designed. The controller has the capability of uniformly treating the hovering and forward flight, and enables a continuous transition between two modes, depending on the velocity command. What is more, by taking rotor thrust and aerodynamic force under consideration simultaneously, a control allocation based on optimization is utilized to realize cooperative control for energy saving. Finally, comprehensive Hardware-In-the-Loop (HIL) simulations are performed to verify the advantages of the designed aircraft and the proposed controller.

Nomenclature

$o_e x_e y_e z_e$	=	Earth-Fixed Coordinate Frame(${}^e\mathcal{F}$)
$o_b x_b y_b z_b$	=	Quadcopter-Body Coordinate Frame(${}^b\mathcal{F}$)
$o_l x_l y_l z_l$	=	Lifting-Wing Coordinate Frame(${}^l\mathcal{F}$)
$o_w x_w y_w z_w$	=	Wind Coordinate Frame(${}^w\mathcal{F}$)
${}^e\mathbf{p}$	=	Position in ${}^e\mathcal{F}$
${}^e\mathbf{v}$	=	Velocity in ${}^e\mathcal{F}$
${}^b\mathbf{v}_a, {}^l\mathbf{v}_a$	=	Airspeed vector in ${}^b\mathcal{F}$ and ${}^l\mathcal{F}$, respectively
${}^e\mathbf{v}_w$	=	Wind velocity in ${}^e\mathcal{F}$
V_a	=	Airspeed

*Corresponding Author, is with the School of Automation Science and Electrical Engineering, Beihang University, Beijing 100191, China.
Email: qq_buaa@buaa.edu.cn.

ϕ, θ, ψ	= Euler angles in ${}^b\mathcal{F}$
$\omega_{x_b}, \omega_{y_b}, \omega_{z_b}$	= Angular velocity in ${}^b\mathcal{F}$
α	= Angle of attack in ${}^1\mathcal{F}$
β	= Sideslip angle in ${}^1\mathcal{F}$
C_L	= Aerodynamic lift coefficient
C_D	= Aerodynamic drag coefficient
C_m	= Aerodynamic pitch moment coefficient
C_Y	= Aerodynamic lateral force coefficient
C_l	= Aerodynamic roll moment coefficient
C_n	= Aerodynamic yaw moment coefficient
κ	= Installation angle of the lifting wing
η	= Installation angle of the motor
c	= Mean chord of the lifting wing
b	= Wingspan of the lifting wing
S	= Area of the lifting wing

I. Introduction

A. Why Lifting-wing Quadcopter

Unmanned aerial vehicles (UAVs) have attracted lots of recent attention due to their outstanding performances in many fields, such as aerial photography, precision farming, and unmanned cargo. According to [1], UAV platforms are currently dominated by three types: fixed-wing UAV, rotorcraft UAV, and their hybrid that integrates the advantages of the first two. The hybrid UAVs have the capability of Vertical Take-off and Landing (VTOL), which enables more accessible grounding or holding by hovering. This might be mandated by authorities in high traffic areas such as lower altitudes in the urban airspace. Furthermore, hybrid UAVs are categorized into two types: convertiplane and tail-sitter. A convertiplane maintains its airframe orientation in all flight modes, but a tail-sitter is an aircraft that takes off and lands vertically on its tail, and the entire airframe needs to tilt nearly 90° to accomplish forward flight [1, 2].

In March 2015, Google announced that the tail-sitter UAV for a packet delivery service was scrapped, because it is still too difficult to control in a reliable and robust manner according to the conclusion came by the project leader [3]. Some studies try to remedy this by newly designed controllers [4]. However, unlike this way, we will study a new type of hybrid UAV, coined as the *lifting-wing quadcopter* [5, 6], to overcome the difficulty Google's Project Wing faced. A lifting-wing quadcopter is a quadcopter [7, 8] with a lifting wing installed at a specific mounting angle. During the flight, the quadcopter will provide thrust upward and forward simultaneously; and the lifting wing also contributes a



Fig. 1 Prototypes of lifting-wing quadcopters.

lifting force partially.

As shown in Fig. 1, as far as we know, some prototypes of lifting-wing quadcopters in public can be found, such as VertiKUL2 by the University of Leuven (Fig. 1 (a), Sept 2015)[9], Vespertilio by the VOLITATION company(Fig. 1 (b))[10], the latest version of the Prime Air delivery drone unveiled by Amazon(Fig. 1(d), Jun 2019)[11] and, RflyLW2 by us(Fig. 1 (c)) [5, 6].

The lifting-wing quadcopter is a new type of hybrid UAV because convertiplane and tail-sitter UAVs in their cruise phase work as fixed-wing UAVs, so the airframe orientation is defined as the head of the fixed-wing. But, the lifting-wing quadcopter is more like a quadcopter. The airframe orientation of the lifting wing needs to tilt a specific angle often within 45° , neither nearly 90° (corresponding to tail-sitter UAVs) nor approximately 0° (corresponding to convertiplane UAVs). Fig. 2 shows the full flight phase of the three VTOL UAVs. The design and performance evaluation of lifting-wing quadcopters have been studied extensively in [5, 6]. In order to make this paper self-contained, we briefly introduce the advantages of the lifting-wing quadcopter compared with some convertiplane and tail-sitter UAVs.

- **Highly reliable structure.** It does not require extra transition actuators. This is a reliable structure by eliminating the need for complicated control.
- **Robust wind resistance.** It has a shorter lifting wing compared with the corresponding fixed wing of convertiplanes and tail-sitter UAVs, because rotors can share the lift. Moreover, as shown in Fig. 4, it does not have a vertical rudder. Instead, this function is replaced by the yaw control of the quadcopter component. In order to improve the

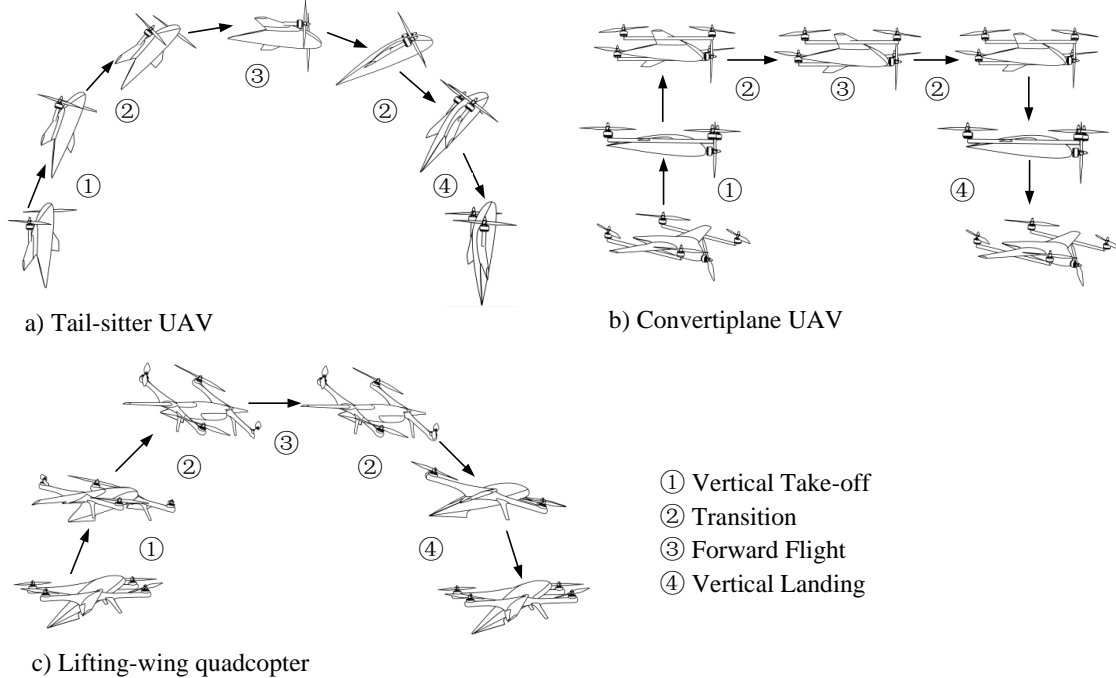


Fig. 2 Different flight modes of some VTOL UAVs.

yaw control ability, the axes of rotors do not point only upward anymore as shown in Fig. 4(a). This implies that the thrust component by rotors can change the yaw directly rather than merely counting on the reaction torque of rotors. From the above, the wind interference is significantly reduced on the one hand; on the other hand, the yaw control ability is improved. As a result, it has better maneuverability and hover control to resist the disturbance of wind than those by tail-sitter and convertiplane UAVs.

- **Low cruise speed.** It can make a cruise at a lower speed than that by convertiplanes and tail-sitter UAVs, meanwhile saving energy compared with corresponding quadcopters. This is very useful when a UAV flies in confined airspace such as a tunnel, where the high speed is very dangerous. Although current hybrid UAVs can have a big or long wing for low cruise speed, they cannot work in many confined airspace due to their long wingspan. However, the lifting-wing quadcopter can be small.
- **Reliable transition flight.** When a tail-sitter UAV performs transition flight, the velocity and angle of attack will change dramatically, leading to complicated aerodynamics even stall. Unlike tail-sitter UAVs, the lifting-wing quadcopter only has to tilt a specific angle often smaller than 45° rather than 90° . The airflow on the lifting wing is stable, and lift and drag are changed linearly with the angle of attack. These will avoid great difficulty (or say danger) in controlling within the full flight envelope.

With the four features above, it is potential for the lifting-wing quadcopter to work fully-autonomously outdoors or in some confined airspace indoors replacing with corresponding quadcopters. The further comparisons with multicopter,

Table 1 Comparison of different VTOL UAVs.

	Endurance	Reliability	Wind Resistance at Hover	Flight Range
Multicopter tilt-rotor/wing convertiplane	4	2	2	4
Multicopter dual-system convertiplane	3	4	2	3
Multicopter tail-sitter	4	4	1	4
Lifting-wing multicopter	2	4	4	2
Multicopter	1	5	5	1

Note: bigger number implies better.

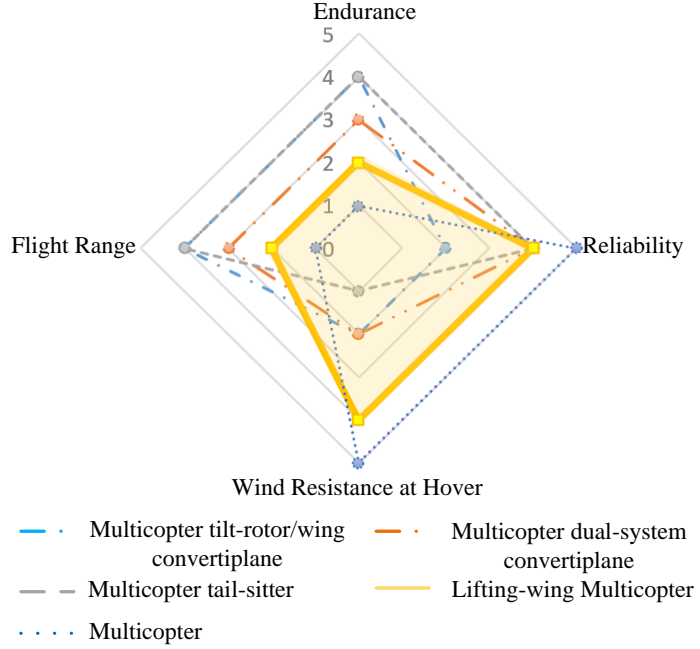


Fig. 3 Comparison of different VTOL UAVs.

tilt-rotor/wing convertiplane, multicopter dual-system convertiplane and multicopter tail-sitter [2] are summarized in Tab. 1 and Fig. 3. As shown, the lifting-wing quadcopter possesses the feature between current hybrid UAVs and quadcopters, and it is more like a quadcopter.

B. Control of Current Hybrid UAVs

The control of the lifting-wing quadcopter has the following two distinguishing features.

- **Unified control for full flight phases.** Hybrid UAVs often have three different flight modes, including the hover, the transition flight, and the forward flight. By taking the multicopter tilt-rotor/wing convertiplane, multicopter dual-system convertiplane and multicopter-tail sitter, for example, their take-off and landing are controlled only by the quadcopter component, while the forward flight is controlled like a fixed-wing aircraft. The two control ways are very different, so the transition flight is challenging due to the nonlinearities and uncertainties. However, a full flight phase of the lifting-wing quadcopter always involves thrust by the quadcopter and aerodynamic force by the

lifting wing. Therefore, the lifting-wing quadcopter can be considered under only the transition flight mode in the full flight phase (hover control here also will take the aerodynamic force into consideration due to wind on the lifting wing). As a result, a unified control is needed. Fortunately, the lifting-wing quadcopter only needs to tilt a specific angle often smaller than 45° , rather than 90° like tail sitter UAVs. This reduces the possibility of having a stall.

- **Cooperative control for energy saving.** The transition flight for current hybrid UAVs is very short, so not too much attention needs to pay to energy consumption in practice. However, it should be considered for the lifting-wing quadcopter as it is under the transition flight mode in the full flight phase. Cooperative control for energy saving is feasible. For example, roll control can be performed by both the quadcopter component and the ailerons by the lifting wing. Obviously, the aileron control is more energy-saving.

Among the control phase of a hybrid UAV, the transition control is the most challenging issue [12], especially for tail-sitter UAVs. Since the actuators of tail-sitter UAVs are like those of lifting-wing quadcopters, the existing transition control of tail-sitter UAVs can be used for reference.

(i) **Trajectory open-loop control for transition flight.**

The open-loop trajectory tracking control is very straightforward. The principle is to make the UAV enter into another mode's condition by focusing on controlling some variables like altitude other than the trajectory, then switch to the controller of the next mode. For example, increasing thrust and reducing its pitch angle at the same time can make a tail-sitter UAV enter into forwarding flight [13, 14]. The aim is to keep the altitude the same [14]. Because the transition time for tail-sitter UAVs is short, the trajectory will not change too much. Obviously, this method is inapplicable to lifting-wing quadcopters.

(ii) **Trajectory closed-loop control for transition flight.**

- *Linearization method based on optimization.* According to the trajectory and the model, the reference state and feedforward are derived by optimization in advance [15, 16]. Based on them, the linearization can be performed. With the resulting linear model, existing controllers against uncertainties and disturbance are designed [17, 18]. As for the lifting-wing quadcopter, this method is applicable when the model and transition trajectory are known prior. Furthermore, cooperative control of the quadcopter component or the ailerons of the lifting wing can be performed by taking energy-saving into optimization. However, in practice, the model is often uncertain as the payload is often changed, such as parcel delivery. Also, this method is not very flexible due to that the trajectory has to be known a priori.
- *Nonlinear control method.* One way is to take all aerodynamic forces as disturbances, and only the quadcopter component works for the flight transition [19, 20]. This requires that the quadcopter has a strong control ability to reject the aerodynamic force. Another way takes the aerodynamic force into consideration explicitly to generate a proper attitude [21, 22]. How to cooperatively control the

quadcopter component and the actuators of fixed-wing is not found so far. This is because, we guess, the transition flight is often short, and more attention is paid to making the UAV stable by reducing the possibility of stall rather than optimization.

As shown above, the linearization method based on optimization is somewhat not flexible, but cooperative control for energy saving can be performed in an open-loop manner. The nonlinear control method is flexible but not considering how to control cooperatively for energy saving.

C. Our Work and Contributions

In this paper, we will consider designing a unified controller for the full flight phase of a lifting-wing quadcopter. What is more, the quadcopter component and the ailerons of the lifting wing work cooperatively to save energy. First, we build the model of the lifting-wing quadcopter. Unlike the tail-sitter UAV, it does not have a rudder, and its tilted rotors will generate force components on the XY-plane in the quadcopter-body coordinate frame (traditional quadcopters do not have the force component on the XY-plane). Because of this, the translational dynamic involves five control variables, namely three-dimensional force in the quadcopter-body coordinate frame and two Euler angles (pitch and roll angles), further by considering the aerodynamic force determined by Euler angles. However, it is difficult and a bit too early to determine the five control variables according to the three-dimensional desired acceleration, because it is hard to obtain the bounds of these control variables. An improper choice may not be realized by actuators. To this end, we only choose the $o_b z_b$ force (the main force component) in the quadcopter-body coordinate frame and two Euler angles (pitch and roll angles) to determine the desired acceleration uniquely, leaving the other two force components as a lumped disturbance. This adopts the controlling idea of quadcopters [7, 23], but the computation method is different due to the existence of the aerodynamic force. With the determined Euler angles, moments are further determined in the lifting wing coordinate frame. So far, the unified control for the full flight phase is accomplished. Finally, we will utilize the control allocation to realize cooperative control for energy saving. The $o_b z_b$ force and three-dimensional moments will be realized by four rotors and two ailerons. This is why we have the freedom to optimize the allocation for saving energy. The principle behind this is to make the aerodynamic force (two ailerons) undertake the control task as much as possible because aileron control is more energy-saving than rotor control. As a result, cooperative control for energy saving is accomplished.

The contributions of this paper are: (i) establish the model of a lifting-wing quadcopter *for the first time*; (ii) a unified controller design for the full flight phase of the lifting-wing quadcopter; (iii) control allocation for energy-saving performance. Comprehensive HIL simulation experiments are performed to show (i) the proposed lifting-wing quadcopter is more energy-saving with aileron; (ii) synthesizing the angular rate command from the coordinated turn in high-speed flight can reduce sideslip; (iii) the transition phase of the proposed lifting-wing quadcopter is significantly better than the tail-sitter and UAVs.

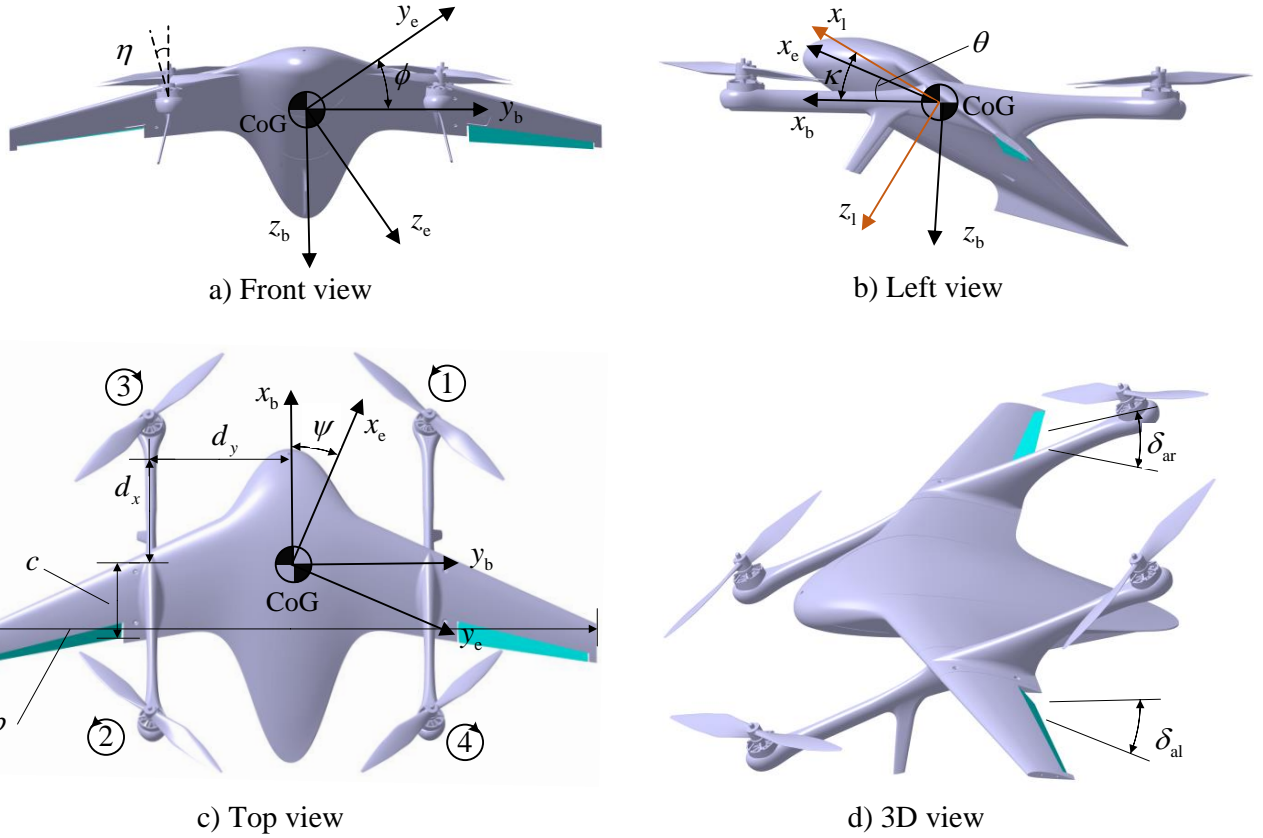


Fig. 4 Coordinate frames and nomenclatures.

II. Coordinate Frame

A lifting-wing quadcopter is divided into two components, the lifting-wing component and the quadcopter component as shown in Fig. 4. According to these, the following coordinate frames are defined.

A. Earth-Fixed Coordinate Frame (${}^e\mathcal{F}$)

The earth-fixed coordinate frame $o_e x_e y_e z_e$ is an inertial frame. The $o_e z_e$ axis points perpendicularly to the ground, and the $o_e x_e$ axis points to a certain direction in the horizontal plane. Then, the $o_e y_e$ axis is determined according to the right-hand rule. This frame is fixed, the initial position of the lifting-wing quadcopter or the center of the Earth is often set as the coordinate origin o_e .

B. Quadcopter-Body Coordinate Frame (${}^b\mathcal{F}$)

The quadcopter-body coordinate frame $o_b x_b y_b z_b$ is fixed to the quadcopter component of a lifting-wing quadcopter. The Center of Gravity (CoG) of the lifting-wing quadcopter is chosen as the origin o_b of ${}^b\mathcal{F}$. The $o_b x_b$ axis points to the nose direction in the symmetric plane of the quadcopter. The $o_b z_b$ axis is in the symmetric plane of the quadcopter, pointing downward, perpendicular to the $o_b x_b$ axis. The $o_b y_b$ axis is determined according to the right-hand rule.

C. Lifting-Wing Coordinate Frame (${}^1\mathcal{F}$)

The lifting-wing coordinate frame $o_l x_l y_l z_l$ is fixed to the lifting-wing component. The origin o_l of ${}^1\mathcal{F}$ is also set at the CoG of the lifting-wing quadcopter. The $o_l x_l$ axis is in the symmetric plane pointing to the nose of the lifting wing. The $o_l z_l$ axis is in the symmetric plane of the lifting wing, pointing downward, perpendicular to the $o_l x_l$ axis, and the $o_l y_l$ axis is determined according to the right-hand rule. The installation angle of the lifting wing, that is the angle between the $o_l x_l$ axis and the $o_l x_l y_l$ plane, is denoted by $\kappa \in \mathbb{R}$ as shown in Fig. 4(b).

D. Wind Coordinate Frame (${}^w\mathcal{F}$)

The origin o_w of the wind coordinate frame $o_w x_w y_w z_w$ is also at the CoG of the lifting-wing quadcopter. The $o_w x_w$ axis is aligned with the airspeed vector. The $o_w z_w$ axis is in the symmetric plane of the lifting wing, pointing downward, perpendicular to the $o_w x_w$ axis, and the $o_w y_w$ axis is determined according to the right-hand rule. The angle of attack (AoA), denoted by $\alpha \in \mathbb{R}$, is defined as the angle between the projection of the airspeed vector on the $o_l x_l z_l$ plane and the $o_l x_l$ as shown in Fig. 4(b). The sideslip angle, denoted by $\beta \in \mathbb{R}$, is defined as the angle between the airspeed vector and the $o_l x_l z_l$ plane as shown in Fig. 4(c).

To convert the aerodynamic forces and moments acting on frame ${}^w\mathcal{F}$ and ${}^1\mathcal{F}$ to ${}^b\mathcal{F}$ respectively, two rotation matrices are defined as followed:

$$\mathbf{R}_w^b(\lambda) = \begin{bmatrix} \cos \lambda \cos \beta & -\cos \lambda \sin \beta & \sin \lambda \\ \sin \beta & \cos \beta & 0 \\ -\sin \lambda \cos \beta & \sin \lambda \sin \beta & \cos \lambda \end{bmatrix}, \mathbf{R}_l^b = \begin{bmatrix} \cos \kappa & 0 & \sin \kappa \\ 0 & 1 & 0 \\ -\sin \kappa & 0 & \cos \kappa \end{bmatrix},$$

where $\lambda = \kappa - \alpha$. And the rotation matrix \mathbf{R}_b^e maps a vector from frame ${}^b\mathcal{F}$ to ${}^e\mathcal{F}$, defined by

$$\mathbf{R}_b^e = \begin{bmatrix} \cos \theta \cos \psi - \sin \theta \sin \phi \sin \psi & -\sin \psi \cos \phi & \cos \psi \sin \theta + \cos \theta \sin \phi \cos \psi \\ \sin \theta \sin \phi \cos \psi + \cos \theta \sin \psi & \cos \phi \cos \psi & \sin \psi \sin \theta - \cos \phi \cos \theta \sin \phi \\ -\cos \phi \sin \theta & \sin \phi & \cos \phi \cos \theta \end{bmatrix}.$$

III. MODELING

A. Assumptions

For the sake of model simplicity, the following assumptions are made:

Assumption 1. The body structure is rigid and symmetric about the $o_l x_l y_l$ plane.

Assumption 2. The mass and the moments of inertia are constant.

Assumption 3. The geometric center of the lifting-wing quadcopter is the same as the CoG.

Assumption 4. The aircraft is only subjected to gravity, aerodynamic forces, and the forces generated by rotors.

B. Flight Control Rigid Model

By **Assumptions 1-2**, the Newton's equation of motion is applied to get the translational motion as follows

$$\begin{aligned} {}^e\dot{\mathbf{p}} &= {}^e\mathbf{v} \\ {}^e\dot{\mathbf{v}} &= \mathbf{R}_b^e \frac{{}^b\mathbf{f}}{m} \end{aligned} \quad (1)$$

where ${}^e\mathbf{p} = [p_{x_e} \ p_{y_e} \ p_{z_e}]^T$ and ${}^e\mathbf{v} = [v_{x_e} \ v_{y_e} \ v_{z_e}]^T$ are the position and velocity expressed in frame ${}^e\mathcal{F}$ respectively; m is the mass, ${}^b\mathbf{f}$ is the total force acting on the airframe expressed in frame ${}^b\mathcal{F}$.

To facilitate attitude control and combine the control characteristics of the rotor and lifting wing, the rotational dynamics is carried out in frame ${}^l\mathcal{F}$. It is given by Euler's equation of motion as

$$\begin{aligned} \dot{\mathbf{R}}_l^e &= \mathbf{R}_l^e [{}^l\boldsymbol{\omega}]_x \\ \mathbf{J} \cdot {}^l\dot{\boldsymbol{\omega}} &= {}^l\mathbf{m} - {}^l\boldsymbol{\omega} \times (\mathbf{J} \cdot {}^l\boldsymbol{\omega}) \end{aligned} \quad (2)$$

where the rotational matrix is derived by $\mathbf{R}_l^e = \mathbf{R}_b^e \mathbf{R}_l^b$, \mathbf{R}_l^b being a constant matrix; ${}^l\mathbf{m}$ is the total moment acting on the airframe expressed in frame ${}^l\mathcal{F}$, ${}^l\boldsymbol{\omega} = [\omega_{x_l} \ \omega_{y_l} \ \omega_{z_l}]^T$ is the angular velocity in frame ${}^l\mathcal{F}$, $[{}^l\boldsymbol{\omega}]_x$ denotes the skew-symmetric matrix

$$[{}^l\boldsymbol{\omega}]_x = \begin{bmatrix} 0 & -\omega_{z_l} & \omega_{y_l} \\ \omega_{z_l} & 0 & -\omega_{x_l} \\ -\omega_{y_l} & \omega_{x_l} & 0 \end{bmatrix},$$

and $\mathbf{J} \in \mathbb{R}^{3 \times 3}$ is the inertia matrix given by

$$\mathbf{J} = \begin{bmatrix} J_x & 0 & -J_{xz} \\ 0 & J_y & 0 \\ -J_{xz} & 0 & J_z \end{bmatrix}.$$

C. Forces and Moments

By **Assumptions 3-4**, the total forces and moments acting on the UAV are decomposed into three parts: the aerodynamic forces and moments acting on the airframe (\mathbf{f}_a and \mathbf{m}_a), the forces and moments generated by rotors (\mathbf{f}_r and \mathbf{m}_r), and the gravitational forces \mathbf{f}_g , where $\mathbf{f}_g = [0 \ 0 \ g]^T$, g is the gravitational acceleration. The front two types of forces and moments will be described detailly in the following two subsections.

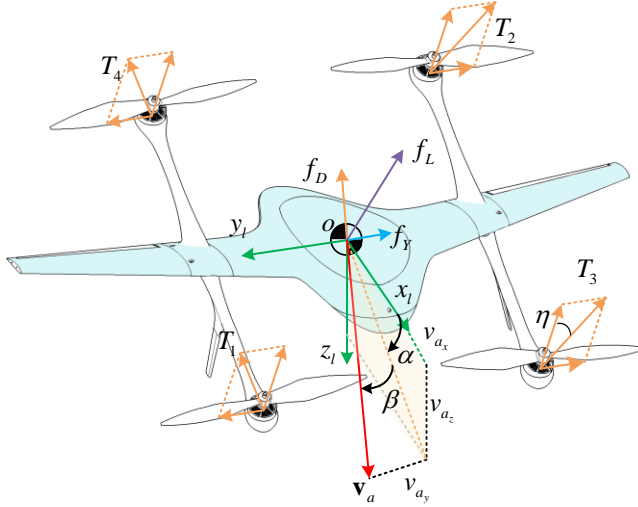


Fig. 5 Forces act on a lifting-wing quadcopter.

1. Forces and Moments in the Quadcopter Component

In the quadcopter part, the thrust and torque produced by one rotor are given by

$$T_i = K_f \varpi_i^2, M_i = K_m \varpi_i^2 = \frac{K_m}{K_f} T_i \quad (3)$$

where $K_f > 0$ is the lift force coefficient, $K_m > 0$ is the drag torque coefficient, and ϖ_i is the angular rate of the i th rotor, $i = 1, 2, 3, 4$. In order to improve the controllability during performing yaw, an installation angle η is set as shown in Fig. 4(a). The left motors tilt to the positive left and right motors tilt to the positive right.

Because of the installation angle η , the forces and moments produced by rotors are expressed by the thrust on each propeller T_i as

$$\begin{bmatrix} f_{r_y} \\ f_{r_z} \\ m_{r_x} \\ m_{r_y} \\ m_{r_z} \end{bmatrix} = \begin{bmatrix} \sin \eta & -\sin \eta & -\sin \eta & \sin \eta \\ -\cos \eta & -\cos \eta & -\cos \eta & -\cos \eta \\ -d_y \cos \eta & d_y \cos \eta & d_y \cos \eta & -d_y \cos \eta \\ d_x \cos \eta & -d_x \cos \eta & d_x \cos \eta & -d_x \cos \eta \\ K_1 & K_1 & -K_1 & -K_1 \end{bmatrix} \begin{bmatrix} T_1 \\ T_2 \\ T_3 \\ T_4 \end{bmatrix}, \quad (4)$$

where $K_1 = K_m / K_f + d_x \sin \eta$, d_x and d_y are the components of the distance from the center of the lifting-wing quadcopter to a propeller on the $o_b x_b y_b$ plane, as shown in Fig. 4(c).

2. Forces and Moments in the Lifting-wing Component

The aerodynamic forces and moments acting on the lifting wing are mainly generated by the lifting wing itself and the ailerons at the trailing edge, as shown in Fig. 5.

Let ${}^e\mathbf{v}_w$ be the wind velocity in ${}^e\mathcal{F}$. Then

$${}^b\mathbf{v}_a = {}^b\mathbf{v} - ({}^b\mathbf{R}_b^e)^T \cdot {}^e\mathbf{v}_w. \quad (5)$$

Thus, the airspeed vector ${}^1\mathbf{v}_a = [v_{a_x} \ v_{a_y} \ v_{a_z}]^T$ and airspeed V_a are defined as

$${}^1\mathbf{v}_a = ({}^b\mathbf{R}_l^b)^T \cdot {}^b\mathbf{v}_a, \quad (6)$$

$$V_a = \sqrt{v_{a_x}^2 + v_{a_y}^2 + v_{a_z}^2}. \quad (7)$$

The aerodynamic angles α and β are defined as

$$\alpha = \tan^{-1}\left(\frac{v_{a_z}}{v_{a_x}}\right), \beta = \sin^{-1}\left(\frac{v_{a_y}}{V_a}\right). \quad (8)$$

In the longitudinal plane, lift, drag, and pitching moment acting on the lifting-wing body are given by

$$\begin{aligned} f_L &= QS(C_L + C_{L\delta_e}\delta_e) \\ f_D &= QS(C_D + C_{D\delta_e}\delta_e) \\ m &= QSc(C_m + C_{m\delta_e}\delta_e). \end{aligned} \quad (9)$$

The lateral force and the roll and yaw moments acting on the lifting-wing body are given by

$$\begin{aligned} f_Y &= QS(C_Y + C_{Y\delta_a}\delta_a) \\ l &= QSb(C_l + C_{l\delta_a}\delta_a) \\ n &= QSb(C_n + C_{n\delta_a}\delta_a) \end{aligned} \quad (10)$$

where $Q = \frac{1}{2}\rho V_a^2$; C_L, C_D, C_m, C_Y, C_l and C_n are nondimensional aerodynamic coefficients, $C_{L\delta_e}, C_{m\delta_e}, C_{D\delta_e}, C_{Y\delta_a}, C_{n\delta_a}$ and $C_{l\delta_a}$ are control derivative; S is the area of the lifting wing, c is the mean chord of the lifting wing, b is the wingspan of the lifting-wing aircraft, δ_e and δ_a are calculated using the right and the left aileron (δ_{ar} and δ_{al} , as shown in Fig. 4(d)) as

$$\begin{bmatrix} \delta_e \\ \delta_a \end{bmatrix} = \begin{bmatrix} 1 & 1 \\ -1 & 1 \end{bmatrix} \begin{bmatrix} \delta_{ar} \\ \delta_{al} \end{bmatrix}. \quad (11)$$

The external forces and moments are summarized as

Table 2 Lifting-wing quadcopter structure parameters, lift force and drag torque coefficients

m	Aircraft mass	1.92 kg
κ	Installation angle of lifting wing	34 deg
η	Installation angle of motor	10 deg
d_x	The distance from $o_b x_b$ to a propeller	0.25 m
d_y	The distance from $o_b y_b$ to a propeller	0.2125 m
$[J_{xx} \ J_{yy} \ J_{zz}]$	Moment of inertia	$[5.12 \ 5.54 \ 7.6] \times 10^{-2} \text{ kg} \cdot \text{m}^2$
b	Wingspan of the lifting-wing aircraft	0.94 m
c	Mean chord of the lifting wing	0.17 m
K_m	Drag moment coefficient	5.875e-07 kg · m ²
K_f	Lift force coefficient	2.824e-05 kg · m ²

$${}^b\mathbf{f} = \begin{bmatrix} 0 \\ f_{r_y} \\ f_{r_z} \end{bmatrix} + QS \mathbf{R}_w^b \begin{bmatrix} -(C_D + C_D \delta_e \delta_e) \\ (C_Y + C_Y \delta_a \delta_a) \\ -(C_L + C_L \delta_e \delta_e) \end{bmatrix} + m \mathbf{R}_e^b \mathbf{f}_g \quad (12)$$

$${}^l\mathbf{m} = \mathbf{R}_b^l \begin{bmatrix} m_{r_x} \\ m_{r_y} \\ m_{r_z} \end{bmatrix} + QS \begin{bmatrix} b(C_l + C_l \delta_a \delta_a) \\ c(C_m + C_m \delta_e \delta_e) \\ b(C_n + C_n \delta_a \delta_a) \end{bmatrix}. \quad (13)$$

The structure parameters, lift force and drag torque coefficients of the lifting-wing quadcopter are given in Tab.2.

IV. CONTROLLER DESIGN

The successive loop closure is a common control architecture for UAVs [24], which consists of an outer-loop controlling the position and an inner-loop for attitude, as illustrated in Fig. 6. The basic idea behind successive loop closure is to close several simple feedback loops in succession around the open-loop plant dynamics rather than designing a single control system. The position controller receives the desired position and then computes the desired acceleration. Then the desired acceleration is mapped to the collective thrust and attitude. The attitude command is sent to the inner-loop, while the thrust command skips directly to the control allocation. To facilitate the control experiment step by step, the attitude can also be commanded by the pilot. Furthermore, the attitude controller receives the desired attitude and generates the desired moment. Finally, the control allocation algorithm distributes the moment command from the inner-loop and the direct force command from the outer-loop to corresponding ailerons and rotors.

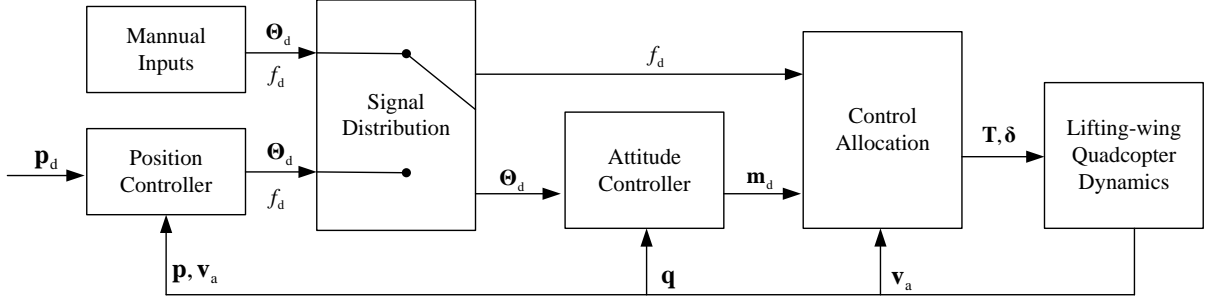


Fig. 6 Control structure

A. Controller Design Model

Since α, β are not easy to obtain, we consider that $\alpha \approx \kappa + \theta$ and $\beta \approx 0$. The translational dynamic involves five control variables, namely three-dimensional forces in frame ${}^b\mathcal{F}$ and two Euler angles (pitch and roll angles). However, it is a bit too early to determine the five control variables according to the three-dimensional desired acceleration because it is hard to obtain the bounds of these control variables. An improper choice may not be realized by ailerons. To this end, we only choose f_z (the main force component) in frame ${}^b\mathcal{F}$ and two Euler angles (pitch and roll angles) to determine the desired acceleration uniquely, and the desired yaw angle is directly specified, leaving f_y as a disturbance. This adopts the controlling idea of quadcopters[7, 23], but the computation method is different due to the existence of the aerodynamic force. According to the idea above, we rewrite the system Eqs. (1) and (2) in the form as

$$\begin{aligned}
 {}^e\dot{\mathbf{p}} &= {}^e\mathbf{v} \\
 {}^e\dot{\mathbf{v}} &= \mathbf{u} + \mathbf{g} + \mathbf{d}_1 \\
 \dot{\mathbf{R}}_l^e &= \mathbf{R}_l^e [{}^l\boldsymbol{\omega}]_x \\
 {}^l\dot{\boldsymbol{\omega}} &= \mathbf{J}^{-1} \cdot {}^l\mathbf{m} + \mathbf{d}_2
 \end{aligned} \tag{14}$$

Here

$$\mathbf{u} = \frac{\mathbf{R}_b^e}{m} \left(\begin{bmatrix} 0 \\ 0 \\ -f_z \end{bmatrix} + Q S \mathbf{R}_w^b \begin{bmatrix} -C_D \\ 0 \\ -C_L \end{bmatrix} \right),$$

and $\mathbf{d}_1, \mathbf{d}_2$ are disturbances, where

$$\begin{aligned}
 \mathbf{d}_1 &= \frac{\mathbf{R}_b^e}{m} \left(\begin{bmatrix} 0 \\ f_y \\ 0 \end{bmatrix} + Q S \mathbf{R}_w^b \begin{bmatrix} -C_D \delta_e \\ (C_Y + C_{Y\delta_a} \delta_a) \\ -C_L \delta_e \end{bmatrix} \right) \\
 \mathbf{d}_2 &= -\mathbf{J}^{-1} \cdot {}^l\boldsymbol{\omega} \times (\mathbf{J} \cdot {}^l\boldsymbol{\omega}).
 \end{aligned}$$

B. Position Control

Given a twice differentiable trajectory $\mathbf{p}_d(t)$, in order to satisfy $\lim_{t \rightarrow \infty} \|\mathbf{p}^e(t) - \mathbf{p}_d(t)\| = 0$, the desired \mathbf{u}_d for Eq. (14) can be designed as a PID controller in the form

$$\mathbf{u}_d = -\mathbf{g} + \ddot{\mathbf{p}}_d - \mathbf{K}_{\mathbf{p}_d} (\mathbf{v}^e - \dot{\mathbf{p}}_d) - \mathbf{K}_{\mathbf{p}_p} (\mathbf{p}^e - \mathbf{p}_d) - \mathbf{K}_{\mathbf{p}_i} \int (\mathbf{p}^e - \mathbf{p}_d) \, ds \quad (15)$$

where $\mathbf{K}_{\mathbf{p}_p}, \mathbf{K}_{\mathbf{p}_i}, \mathbf{K}_{\mathbf{p}_d} \in \mathbb{R}^{3 \times 3}$ are diagonal matrices acting as control gains. The left work is to determine desired thrust by rotors $f_d \in \Omega_f$ and $\theta_d, \phi_d \in \Omega_a$ such that

$$(f_d, \theta_d, \phi_d) = \arg \min_{f_z \in \Omega_f, \theta, \phi \in \Omega_a} \|\mathbf{u}(f_z, \theta, \phi) - \mathbf{u}_d\| \quad (16)$$

where Ω_f is a set to confine the force, and Ω_a is a set to confine the pitch and roll. In order to reduce drag, the vehicle's nose should be consistent with the current direction of the vehicle velocity, that is

$$\psi_d = \tan^{-1} \left(\frac{v_{y_e}}{v_{x_e}} \right). \quad (17)$$

The attitude command can also be given by the pilot, in case the position controller fails with GPS denied, as shown in Fig. 6. Finally, the desired attitude is given as $\Theta_d = [\phi_d \ \theta_d \ \psi_d]^T$.

C. Attitude Control

The attitude controller generates the desired moment from the output of the position controller or the attitude given by the pilot, as shown in Fig. 6. As far as we know, studies about the hybrid UAV hardly consider the lateral control, such as turning right or left. As for the considered UAV, the control on yaw is quite different between the multicopter mode and the fixed-wing mode. To establish a unified control, the attitude control is performed on the lifting-wing frame ${}^1\mathcal{F}$, so ${}^1\Theta_d = [\phi_d \ \theta_d + \kappa \ \psi_d]^T$.

1. Basic Attitude Control

The attitude error is presented in the form of quaternion based on which the corresponding controller is designed. This can guarantee a uniform and good convergence rate for all initial attitude errors [25]

$$\mathbf{q}_e = \mathbf{q}_d^* \otimes \mathbf{q}_l^e = [q_{e_0} \ q_{e_1} \ q_{e_2} \ q_{e_3}]^T, \quad (18)$$

where \mathbf{q}_d is transformed from ${}^1\Theta_d$ with ‘ZXY’ rotational sequence, $(\cdot)^*$ is the conjugate of a quaternion, and \otimes is the quaternion product. Then \mathbf{q}_e is transformed into the axis-angle form $\mathbf{q}_e = [\cos \frac{\vartheta}{2} \ \boldsymbol{\xi}_e^T \sin \frac{\vartheta}{2}]^T$ by

$$\vartheta = \text{wrap}_\pi(2\text{acos}(\mathbf{q}_{e_0}))$$

$$\boldsymbol{\xi}_e = \begin{cases} [0 \ 0 \ 0]^T, & \theta = 0 \\ \text{sign}(\mathbf{q}_{e_0}) \frac{\vartheta}{\sin \vartheta/2} [q_{e_1} \ q_{e_2} \ q_{e_3}]^T, & \theta \neq 0. \end{cases} \quad (19)$$

The function $\text{wrap}_\pi(\vartheta)$ constrains the ϑ in $[-\pi \ \pi]$ to ensure the shortest rotation path. To eliminate the attitude error, the attitude control is designed as

$${}^1\omega_{ac} = \text{sat}(\mathbf{K}_{\Theta p} \boldsymbol{\xi}_e, \omega_{\min}, \omega_{\max}) \quad (20)$$

where $\mathbf{K}_{\Theta p} \in \mathbb{R}^{3 \times 3}$ is the diagonal matrix acting as the control gain, ω_{\min} and $\omega_{\max} \in \mathbb{R}^3$ are the minimum and maximum angular control rates, the function $\text{sat}(\mathbf{x}, \mathbf{x}_{\min}, \mathbf{x}_{\max})$ is defined as

$$\text{sat}(\mathbf{x}, \mathbf{x}_{\min}, \mathbf{x}_{\max}) \triangleq \begin{bmatrix} \text{sat}(x_1, x_{1,\min}, x_{1,\max}) \\ \vdots \\ \text{sat}(x_n, x_{n,\min}, x_{n,\max}) \end{bmatrix}, \text{sat}(x_k, x_{k,\min}, x_{k,\max}) \triangleq \begin{cases} x_{k,\min}, & x_k < x_{k,\min} \\ x_{k,\max}, & x_k > x_{k,\max} \\ x_k, & \text{else} \end{cases}. \quad (21)$$

2. Lateral Compensation

When the UAV is in high-speed flight, a roll command given to track a specified trajectory will cause a lateral skid. In order to reduce the sideslip angle when the UAV turns at a high speed, the coordinated turn should be considered. In ${}^1\mathcal{F}$ frame, if it is assumed that there is no wind, the coordinated turn equation is expressed as [24]

$$\dot{\psi}_d = \frac{g \tan \phi}{V_a}. \quad (22)$$

It should be noted that the Euler angles are the attitude presentation between ${}^1\mathcal{F}$. So the desired yaw rate generated by coordinated turn is

$${}^1\omega_{ct} = \dot{\psi}_d \cos \theta \cos \phi. \quad (23)$$

3. Angular Rate Command Synthesis

In the lifting-wing coordinated turn, V_a being zero makes no sense. In addition, considering that coordinated turn should not be used when airspeed is small, a weight coefficient related to airspeed is added. So the desired angular rates are rewritten as

$${}^1\omega_d = \left[\omega_{d_{ac,x}} \ \omega_{d_{ac,y}} \ \left(\omega_{d_{ac,z}} + w \cdot {}^1\omega_{ct} \right) \right] \quad (24)$$

where $w = \text{sat}\left(\frac{V_a - V_{\min}}{V_{\max} - V_{\min}}, 0, 1\right)$. When the airspeed is slower than V_{\min} , the desired yaw rate is completely decided by the basic attitude controller. In contrast, when ${}^1\omega_{d_z} = 0$ and the airspeed reaches the specified value V_{\max} , the desired yaw rate is completely decided by the coordinated turn.

4. Attitude Rate Control

To eliminate the attitude rate error, the controller is designed as

$${}^1\mathbf{m}_d = \text{sat}\left(\mathbf{J}(-\mathbf{K}_{\omega_p}({}^1\omega - {}^1\omega_d) - \mathbf{m}_{d,I} - \mathbf{K}_{\omega_d}({}^1\dot{\omega} - {}^1\dot{\omega}_d)), -\mathbf{m}_{d,\max}, \mathbf{m}_{d,\max}\right) \quad (25)$$

where $\mathbf{m}_{d,I} = \text{sat}\left(\mathbf{K}_{\omega_i} \int ({}^1\omega - {}^1\omega_d) ds, -\mathbf{m}_{d,I\max}, \mathbf{m}_{d,I\max}\right)$, \mathbf{K}_{ω_p} , \mathbf{K}_{ω_i} , $\mathbf{K}_{\omega_d} \in \mathbb{R}^{3 \times 3}$ are diagonal matrices acting as control gains, $\mathbf{m}_{d,I\max}$ is maximum amplitude of integral action, $\mathbf{m}_{d,\max}$ is the maximum moment generated by actuators.

So far, we have obtained f_d and ${}^1\mathbf{m}_d$, which will be further realized by $T_1, \dots, T_4, \delta_{ar}, \delta_{al}$.

D. Control Allocation

The lifting-wing quadcopter is an over-actuated aircraft, which provides six independent control inputs, namely $T_1, \dots, T_4, \delta_{ar}, \delta_{al}$ to meet a specific thrust $f_d \in \mathbb{R}$ and moment demand ${}^1\mathbf{m}_d \in \mathbb{R}^3$. A method of control allocation based on optimization is proposed. Recalling the control in translational dynamic, if we determined the three-dimensional force in ${}^b\mathcal{F}$ and two Euler angles (pitch and roll angles) by an optimization before, then the six control variables (plus desired yaw angle) will be determined by six actuators uniquely. If so, however, the optimization in the control of the translational dynamic is not related to energy-saving directly. This is why we only choose the $o_b z_b$ force (the main force component) and two Euler angles (pitch and roll angles) to determine the desired acceleration as in Eq.(16).

First, Eqs. (12) and (13) are rearranged as

$$\underbrace{\begin{bmatrix} f_z \\ {}^1m_x - QScC_l \\ {}^1m_y - QScC_m \\ {}^1m_z - QScC_n \end{bmatrix}}_{\mathbf{u}_v} = \underbrace{\begin{bmatrix} -\cos\eta & -\cos\eta & -\cos\eta & -\cos\eta & 0 & 0 \\ -K_2 & K_3 & K_2 & -K_3 & -QScC_l\delta_a & QScC_l\delta_a \\ d_x \cos\eta & -d_x \cos\eta & d_x \cos\eta & -d_x \cos\eta & QScC_m\delta_e & QScC_m\delta_e \\ -K_5 & K_4 & K_5 & -K_4 & -QScC_n\delta_a & QScC_n\delta_a \end{bmatrix}}_{\mathbf{B}} \underbrace{\begin{bmatrix} T_1 \\ T_2 \\ T_3 \\ T_4 \\ \delta_{ar} \\ \delta_{al} \end{bmatrix}}_{\boldsymbol{\delta}} \quad (26)$$

where $K_2 = d_y \cos\eta \cos\kappa + K_1 \sin\kappa$, $K_3 = d_y \cos\eta \cos\kappa - K_1 \sin\kappa$, $K_4 = d_y \cos\eta \sin\kappa + K_1 \cos\kappa$, $K_5 = d_y \cos\eta \sin\kappa - K_1 \cos\kappa$. The value $\boldsymbol{\delta}$ is the control input of the actuator, \mathbf{u}_v is the virtual control, \mathbf{B} is the control efficiency matrix.

As shown in the Eq.(26), $\text{rank}(\mathbf{B}) = 4$, the dimension of $\boldsymbol{\delta}$ is 6, which is higher than that of \mathbf{u}_v , so Eq.(26) has a minimum norm solution. To take the control priority of the \mathbf{u}_v components, actuator priority of $\boldsymbol{\delta}$ and actuator saturation

under consideration, the control allocation is formulated to be an optimization problem as

$$\begin{aligned} \min \quad & \|\mathbf{W}_u (\mathbf{B}\delta - \mathbf{u}_{v,d})\|^2 + \gamma \|\mathbf{W}_\delta (\delta - \delta_p)\|^2 \\ \text{s.t.} \quad & \underline{\delta} \leq \delta \leq \bar{\delta} \end{aligned} \quad (27)$$

where $\mathbf{u}_{v,d} = [f_d^{-1}m_{d_x} - QSbC_l^{-1}m_{d_y} - QSbC_m^{-1}m_{d_z} - QSbC_n]^T$ is the desired virtual control, δ_p is the preferred control vector which will be specified later, $\mathbf{W}_u \in \mathbb{R}^{6 \times 6}$ is a positive definite weighting matrix that prioritizes the commands in case the desired virtual input $\mathbf{u}_{v,d}$ cannot be achieved, $\mathbf{W}_\delta \in \mathbb{R}^{6 \times 6}$ is a positive definite weighting matrix that prioritizes the different actuators, $\underline{\delta} = \max(\delta_{\min}, \delta_l - \Delta\delta)$, $\bar{\delta} = \min(\delta_{\max}, \delta_l + \Delta\delta)$ are lower and upper bounds at each sampling instant of actuators, δ_{\min} and $\delta_{\max} \in \mathbb{R}^6$ are actuator position limits, $\Delta\delta \in \mathbb{R}^6$ is the rate limit, and δ_l is the last value of δ .

There are two optimization objectives in Eq.(27), namely $\|\mathbf{W}_u (\mathbf{B}\delta - \mathbf{u}_{v,d})\|^2$ and $\|\mathbf{W}_\delta (\delta - \delta_p)\|^2$. The first one is the primary objective of minimizing the slack variables weighted by \mathbf{W}_u , so the weighting factor γ is often chosen to be a small value. In many cases, the preferred control vector is set to the last value of δ , $\delta_p = \delta_l$. But, in order to save energy, we prefer to use the aerodynamic force because the change of rotor force implies the motor's rotational speed change, which is power-hungry. According to the consideration above, we can give more weight to δ_{ar} and δ_{al} and set first four elements of δ_p to $\frac{T_1+T_2+T_3+T_4}{4}$, and last two elements to that of δ_l .

The hardware resources of the flight control are very limited, so it is very important to ensure the real-time operation of the proposed algorithm. Several different algorithms, like redistributed pseudoinverse, interior-point methods, and active set methods have been proposed to solve the constrained quadratic programming problem. Among them, active set methods[26] perform well in the considered control allocation problems, because they have the advantage that their initialization can take advantage of the solution from the previous sample (known as the warm start), which is often a good guess for the optimal solution at the current sample. This can reduce the number of iterations needed to find the optimal solution in many cases. The study [27] shows that the computational complexity of the active set methods is similar to the redistributed pseudoinverse method and the fixed-point algorithm, but the active set methods produce solutions with better accuracy.

V. Simulation Experiments

In order to verify the three main advantages of the designed aircraft: control performance, energy saving and reliable transition flight, several experiments are conducted. The verification of these performances is mainly determined by two factors, namely, with and without ailerons, and with and without coordinated turn.

Therefore, experiments are primarily composed of two parts. One is the comparison of control performance, energy saving and transition flight with and without aileron. And the other is the comparison of control performance with and

without coordinated turn, but both with aileron. In addition, the transition flight of three different VTOL vehicles, as shown in Fig. 2, is analyzed in the HIL simulation environment.

A. Simulation Platform

The HIL simulation is carried out in the RflySim platform [28–30], which provides CopterSim simulator and supports Pixhawk/PX4 autopilot. When perform the HIL simulation, CopterSim sends sensor data such as accelerometer, barometer, magnetometer, which is generated by a mathematical model, to the Pixhawk system via a USB serial port. The Pixhawk/PX4 autopilot will receive the sensors data for state estimation by the EKF2 filter and send the estimated states to the controller through the internal uORB message bus as the feedback. Then the controller sends the control signal of each motor as output back to CopterSim. Thereby a close-loop is established in the HIL simulation. Compared with the numerical simulation, the control algorithm is deployed and run in a real embedded system as the real flight does. After HIL simulation, the controller will be directly deployed to a real vehicle and further verification experiments will be performed.

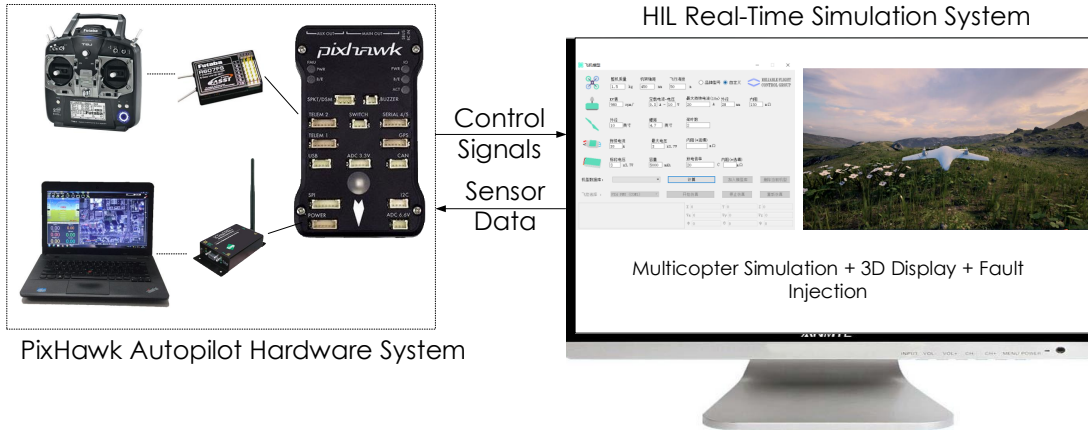


Fig. 7 HIL simulation of RflyLW2.

The lifting-wing quadcopter model is built in MATLAB/Simulink according to Eqs. (1),(2) (12), (13). Besides, the dynamics of the motor and servo are modeled as first-order transfers as follows:

$$\varpi = \frac{1}{T_m s + 1} (C_m \sigma_i + \varpi_b), \delta_a = \frac{1}{T_a s + 1} (C_a \sigma_j + \delta_b), i = 1, 2, 3, 4, j = 5, 6 \quad (28)$$

where $\sigma_i \in [0, 1]$ is i th throttle command, T_m and T_a are the time constant parameter of motor and servo response, C_m , C_a , δ_b and ϖ_b are constant parameters. The sensors used in HIL simulation include IMU, magnetometer, barometer, GPS and airspeed meter, are modeled reference to [7].

Due to the vehicle's VTOL capabilities, the aerodynamic parameters must not only be modeled up to the stall AoA,

but also in the post-stall region, in order to cover the entire flight envelope. The full angle aerodynamic parameters are obtained by combining the small angle aerodynamic parameters obtained by CFD simulation and the empirical aerodynamic model [31]. The aerodynamic characteristics at low and large AoA are approximated as

$$\begin{cases} C_{L_S}(\alpha) = \frac{0.5c_2^2}{(c_2 - c_3)\cos^2(\alpha) + c_3} \sin(2\alpha) \\ C_{D_S}(\alpha) = c_0 + \frac{c_2c_3}{(c_2 - c_3)\cos^2(\alpha) + c_3} \sin^2(\alpha) \end{cases}, \begin{cases} C_{L_L}(\alpha) = c_1 \sin(2\alpha) \\ C_{D_L}(\alpha) = c_0 + 2c_1 \sin^2(\alpha) \end{cases},$$

and a pseudo-sigmoid function

$$\sigma(\alpha_0, k, \alpha) = \frac{1 + \tanh(k\alpha_0^2 - k\alpha^2)}{1 + \tanh(k\alpha_0^2)}, \alpha \in [-\pi, \pi]$$

is used to blend low and large AoA regions together

$$\begin{cases} C_L(\alpha) = C_{L_S}(\alpha) \sigma(\alpha_0, k_L, \alpha) + C_{L_L}(\alpha) [1 - \sigma(\alpha_0, k_L, \alpha)] \\ C_D(\alpha) = C_{D_S}(\alpha) \sigma(\alpha_0, k_D, \alpha) + C_{D_L}(\alpha) [1 - \sigma(\alpha_0, k_D, \alpha)] \end{cases}. \quad (29)$$

The low and large AOA parameters c_0, c_1, c_2, c_3 , and blending parameters α_0, k_L, k_D are turned according to CFD results, and their values are set to $c_0 = 0.055, c_1 = 0.9, c_2 = 13.0, c_3 = 3.3, \alpha_0 = 3\text{deg}, k_L = 38, k_D = 48$. Corresponding Aerodynamic curves are shown in Fig. 8.

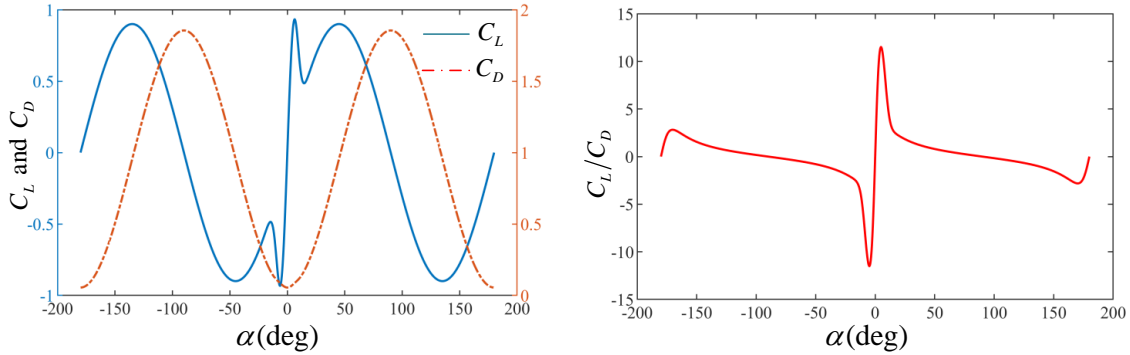


Fig. 8 Aerodynamic parameters obtained by CFD

B. Simulation Experiments

1. Verifying the Effectiveness of Aileron

In order to show the effectiveness of ailerons, two groups of comparative experiments are carried out. The attitude control and position control are the same, but the control allocation of the first group uses the aileron, while the second

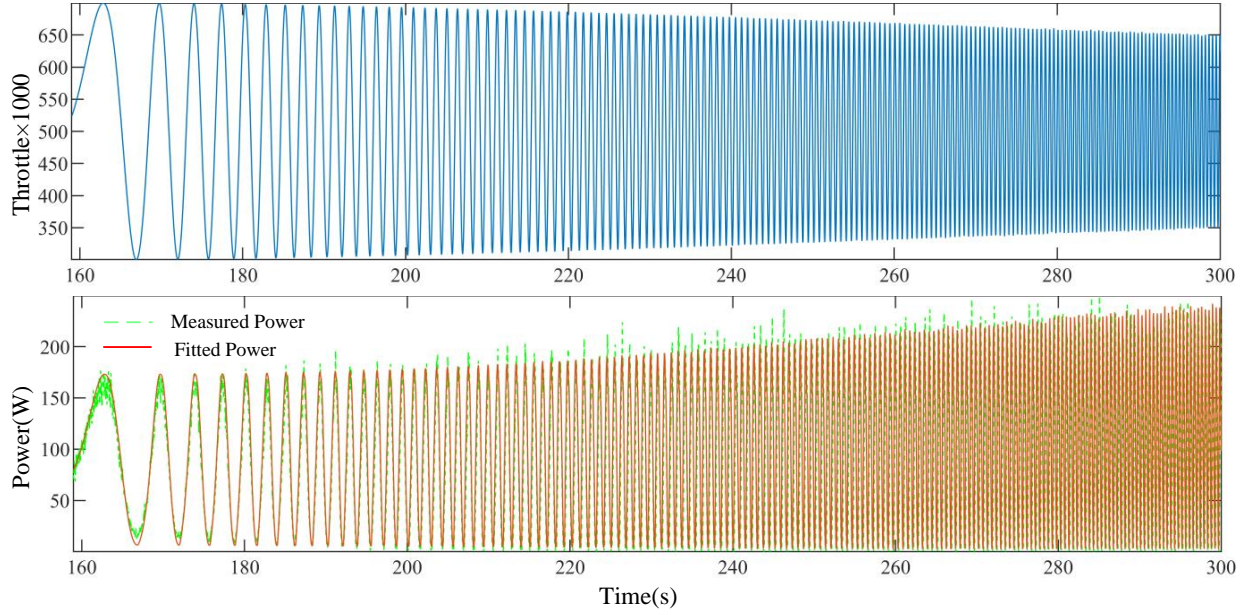


Fig. 9 Throttle command and identification result of the motor

group does not. The second group only depends on the quadcopter control allocation. In this experiment, the aircraft tracks the specified trajectory, as shown in Fig. 10(a), which is a straight line plus a circle with a radius of 200m.

As shown in Fig. 10(b), after adding the aileron, the control amplitude of the four motors is almost the same trend, especially when the aircraft transits between straight and circular trajectories, indicating that the attitude control is mainly realized by the aileron, and motors are more like a thruster on a fixed-wing in this case. However, when the attitude changes sharply, as shown in Fig. 10(b) during $t = 22 \sim 23$ s, the motor and aileron will participate in the control at the same time to improve the control performance. When the state of the UAV is in the slow adjustment, the aileron undertakes the control as much as possible to save energy.

In order to quantify the influence of ailerons, the relationship between throttle command and energy consumption of the motor and actuator is identified. A sinusoidal signal with the constant amplitude and linear increasing frequency is designed, and the energy consumption test experiments are carried out on the servo and motor at the same time. Measurement and identification results of the motor are shown in the Fig.9, in which the amplitude of the throttle decreases as the frequency increasing, because a low-pass filter in Eq.(28) is applied to it. We find that the motor power has a quadratic function relationship with a fixed throttle, and the power is different when the motor accelerates and decelerates. When the change frequency of the throttle command becomes faster, the power is increased. Therefore, the following formula is established to fit the relationship between throttle command and motor power

$$P_T = \sum_{i=1}^4 p_1 \sigma_i^2 + p_2 \sigma_i + p_3 \dot{\sigma}_{up,i}^4 + p_5 \dot{\sigma}_{down,i}^6 + p_7 \quad (30)$$

With the given lifting-wing quadcopter platform, $p_1 = 563.7$, $p_2 = -147.4$, $p_3 = 15$, $p_4 = 1.05$, $p_5 = 4$, $p_6 = 1$, $p_7 = 0.05538$. With respect to the servo, its power is negligible, because the power of servo is only 0.2W, far less than the motor's, even if the 100g weight is suspended on the two ailerons.

The trajectory tracking experiment is performed three times, with the forward flight speed of 5m/s, 10m/s and 20m/s, respectively. The powers in three flight speeds are shown in Fig. 10(c). It can be observed that when the speed is 5m/s, the power is the same, because the aileron is not used at slow flight speed. When the speed increases to 10m/s, the power with the aileron is slightly smaller. Further when the speed increases to 20m/s, the power with the aileron is greatly smaller because the aerodynamic force is stronger at high speed.

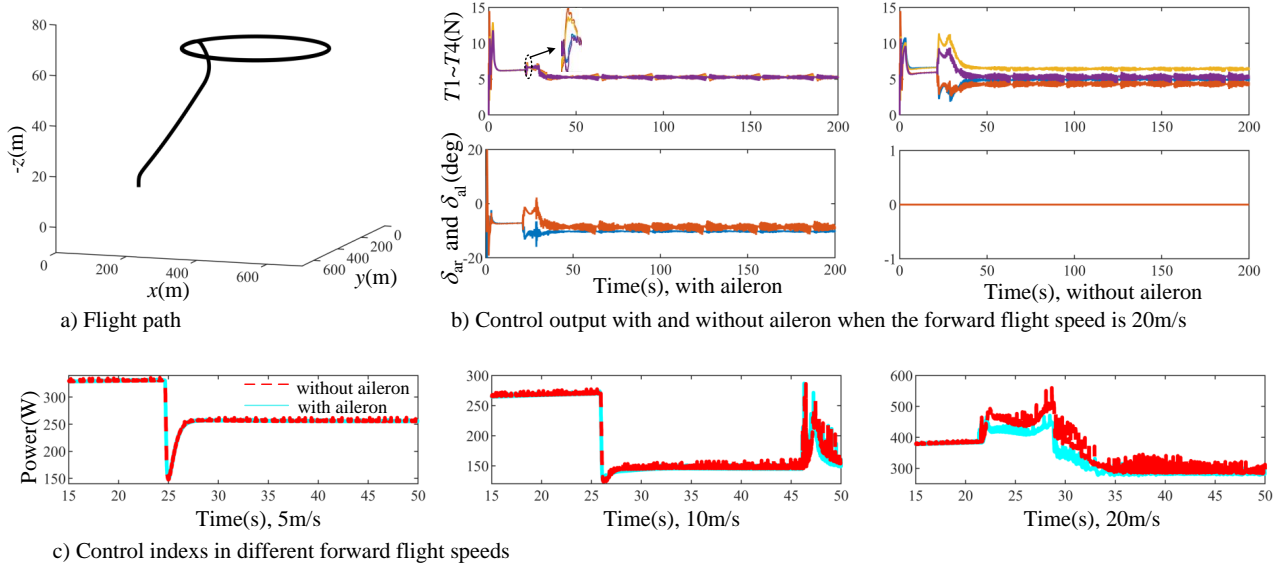


Fig. 10 The attitude control performance and mixer output with and without aileron

2. Verifying the Effectiveness of Coordinated Turn

As for the lateral control, experiments are carried out in hover and high-speed forward flight, and the results are shown in Fig. 11. In the high-speed forward flight, as shown in Fig. 11 yellow region, when a turn command is given for the first time during 30.8 ~ 42.2s, the lifting-wing quadcopter with coordinated turn has no sideslip angle and has a better lateral tracking performance, as shown in Fig.11(a.1 vs. b.1, and a.5 vs. b.5). In this state, the control of the lifting-wing quadcopter is similar to the fixed-wing, and the desired yaw rate is generated by Eq.(23) as the feedforward. When the turn command is given for the second time during 60.8 ~ 72.2s, the lifting-wing quadcopter is in low-speed flight, and the control of the lifting-wing quadcopter is similar to the quadcopter, so a big sideslip angle appears both in experiments with and without coordinated turn.

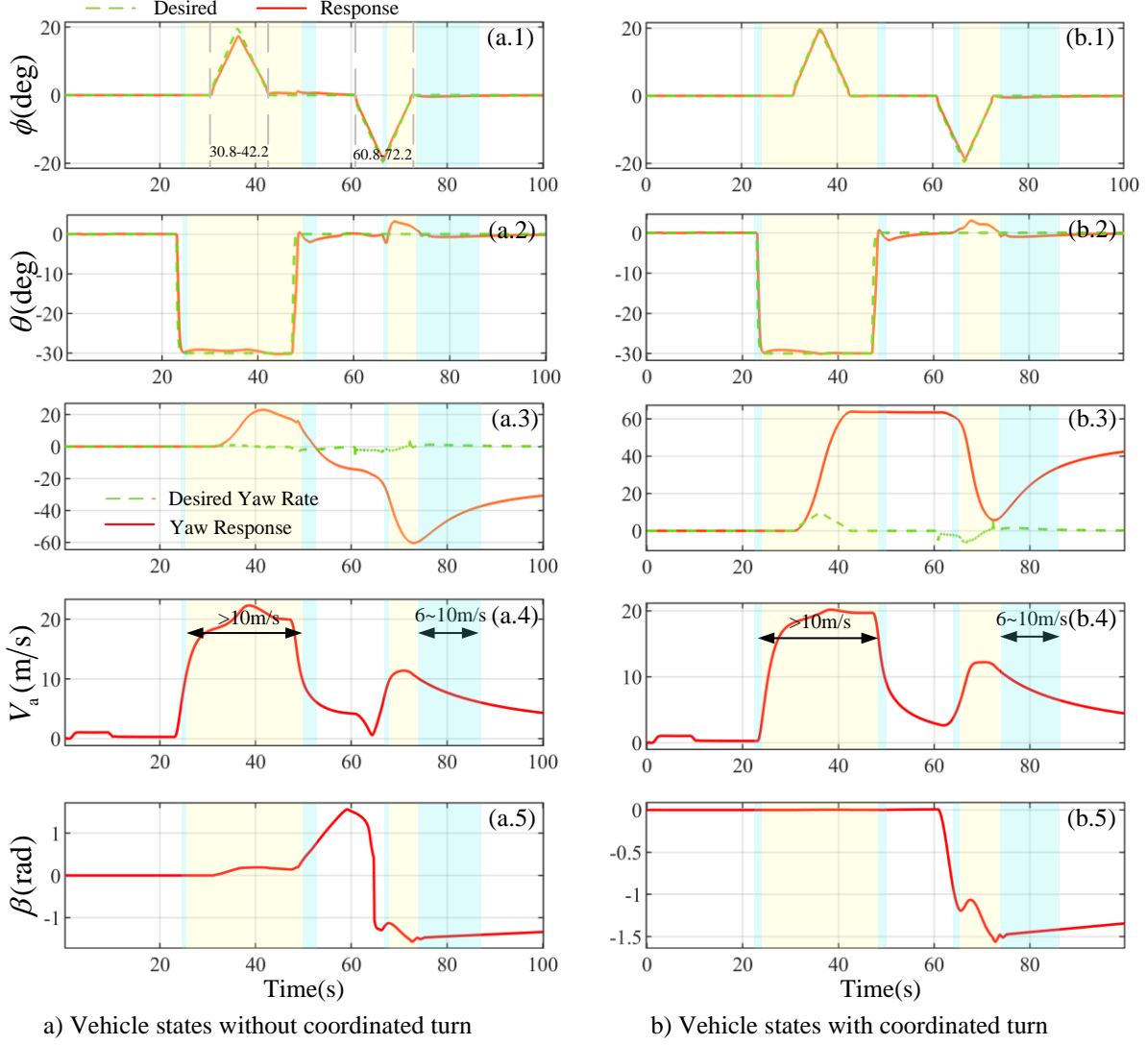


Fig. 11 The control response with and without coordinated turn

3. Transition Flight

The transition flight is often defined as the aircraft changing from hover to level flight. To quantify the phase, the transition process is defined as the time it takes for the aircraft to start a transitional flight to the airspeed greater than 18m/s. The quality of the transition is mainly reflected in the *transition time* and *control accuracy of altitude*. In the simulation, the aircraft will take off to a certain altitude, and then a step signal of -30° is given to the pitch channel. This is because the wind CFD test results show that the maximum energy efficiency is obtained when $\alpha = 4^\circ$. As a comparison, the same experiment is performed on a tail-sitter quadcopter. The model of the tail-sitter quadcopter is built on the lifting-wing quadcopter with the installation angle of the lifting-wing from 34° to 90° , as shown in Fig. 2(a).

Fig.12 shows the response curves of the pitch angle, altitude and airspeed of the lifting-wing quadcopter and tail-sitter UAV in the transition phrase in the HIL simulation. It can be observed that during the transition phase of

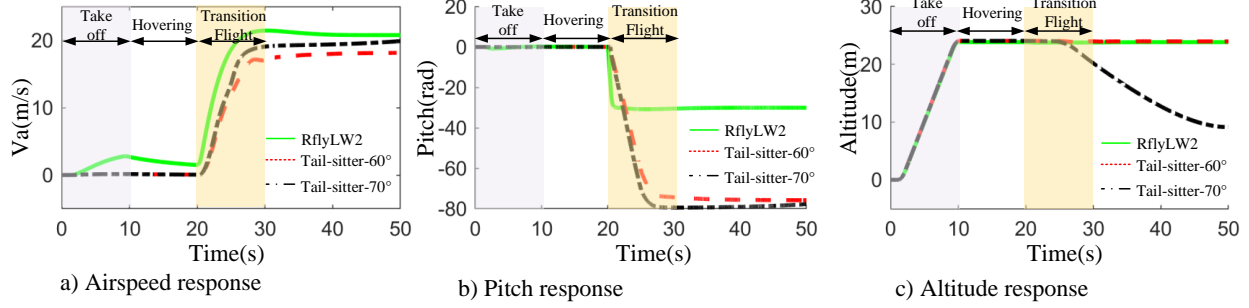


Fig. 12 Transition flight of lifting-wing quadcopter and tail-sitter UAV.

the lifting-wing quadcopter, the time for the pitch angle to reach the desired value is 1.1s, as shown in Fig.12(b), and the time it takes for the airspeed to reach the set 18m/s is 4.7s as shown in Fig.12(a). So the transition time of the lifting-wing quadcopter is 4.7s. Furthermore, the altitude decreases as soon as the transition starts, with a maximum altitude error of 0.09 m at $t = 21.68$ s. As for tail-sitter UAV, the transition time is 7.1s, when the desired pitch angle is -70° . But after the transition, the altitude drops sharply, as shown in Fig.12(c). When the desired pitch angle is -60° , the altitude is stable, but the transition time is 20.48s much longer than that of the RflyLW2. Thus, the transition phase of the lifting-wing quadcopter is significantly better than the tail-sitter UAV, and does not require an additional controller.

VI. Conclusion

The modeling, controller design, and HIL simulation verification of the lifting-wing quadcopter—a novel type of hybrid aircraft—are presented in this paper. The modeling portion takes into account the forces and moments produced by the lifting wing and rotors. A unified controller for the entire flight phase is created based on the existing model. Depending on the velocity command, the controller can regard hovering and forward flight equally and enable a seamless transition between the two modes. The experimental results show that the proposed aircraft outperforms the tail-sitter UAV in terms of tracking performance during the transition phase. In addition, the controller combines the characteristics of the quadcopter and fixed-wing control law, allowing it to retain yaw during the hover phase and decrease sideslip angle during the cruise phase. What is more, a control allocation based on optimization is utilized to realize cooperative control for energy saving, by taking rotor thrust and aerodynamic force under consideration simultaneously. Through identification, we find that compared with the motor, the aileron can reduce the energy consumption when implementing high-frequency control inputs.

References

[1] Saeed, A. S., Younes, A. B., Cai, C., and Cai, G., “A survey of hybrid unmanned aerial vehicles,” *Progress in Aerospace Sciences*, Vol. 98, 2018, pp. 91 – 105.

[2] Raj, N., Banavar, R., Abhishek, and Kothari, M., “Attitude control of a novel tailsitter: swiveling biplane-quadrrotor,” *Journal of Guidance, Control, and Dynamics*, Vol. 43, No. 3, 2020, pp. 599–607.

[3] wsj.com, “Google tail-sitter UAV,” <https://www.wsj.com/articles/BL-DGB-40935>, 2015. Accessed January 1, 2023.

[4] Ritz, R., and D’Andrea, R., “A global strategy for tailsitter hover control,” *Robotics Research*, Springer, 2018, pp. 21–37.

[5] Xiao, K., Meng, Y., Dai, X., Zhang, H., and Quan, Q., “A lifting wing fixed on multirotor UAVs for long flight ranges,” *2021 International Conference on Unmanned Aircraft Systems (ICUAS)*, IEEE, 2021, pp. 1605–1610.

[6] Zhang, H., Tan, S., Song, Z., and Quan, Q., “Performance evaluation and design method of lifting-wing multicopters,” *IEEE/ASME Transactions on Mechatronics*, Vol. 27, No. 3, 2021, pp. 1606–1616.

[7] Quan, Q., *Introduction to multicopter design and control*, Springer, 2017.

[8] Emran, B. J., and Najjaran, H., “A review of quadrotor: An underactuated mechanical system,” *Annual Reviews in Control*, Vol. 46, 2018, pp. 165–180.

[9] Theys, B., De Vos, G., and De Schutter, J., “A control approach for transitioning VTOL UAVs with continuously varying transition angle and controlled by differential thrust,” *2016 international conference on unmanned aircraft systems (ICUAS)*, IEEE, 2016, pp. 118–125.

[10] tx tech.cn, “Volitation vespertilio,” <http://www.tx-tech.cn/en/col.jsp?id=133>, 2019. Accessed January 1, 2023.

[11] theverge.com, “Amazon Prime Air,” <https://www.theverge.com/2019/6/5/18654044/amazon-prime-air-delivery-drone-new-design-safety-transforming-flight-video>, 2019. Accessed January 1, 2023.

[12] Hassanalian, M., and Abdelkefi, A., “Classifications, applications, and design challenges of drones: A review,” *Progress in Aerospace Sciences*, Vol. 91, 2017, pp. 99–131.

[13] Argyle, M. E., Beard, R. W., and Morris, S., “The vertical bat tail-sitter: dynamic model and control architecture,” *2013 American Control Conference*, IEEE, 2013, pp. 806–811.

[14] Escareno, J., Stone, R., Sanchez, A., and Lozano, R., “Modeling and control strategy for the transition of a convertible tail-sitter UAV,” *2007 European Control Conference (ECC)*, IEEE, 2007, pp. 3385–3390.

[15] Oosedo, A., Abiko, S., Konno, A., and Uchiyama, M., “Optimal transition from hovering to level-flight of a quadrotor tail-sitter UAV,” *Autonomous Robots*, Vol. 41, No. 5, 2017, pp. 1143–1159.

[16] Li, B., Sun, J., Zhou, W., Wen, C.-Y., Low, K. H., and Chen, C.-K., “Transition optimization for a VTOL tail-sitter UAV,” *IEEE/ASME Transactions on Mechatronics*, 2020.

[17] Li, B., Sun, J., Zhou, W., Wen, C.-Y., Low, K. H., and Chen, C.-K., “Nonlinear robust flight mode transition control for tail-sitter aircraft,” *IEEE/ASME transactions on mechatronics*, Vol. 25, No. 5, 2020, pp. 2534–2545.

[18] Smeur, E. J., Bronz, M., and de Croon, G. C., “Incremental control and guidance of hybrid aircraft applied to a tailsitter unmanned air vehicle,” *Journal of Guidance, Control, and Dynamics*, Vol. 43, No. 2, 2020, pp. 274–287.

[19] Lyu, X., Gu, H., Zhou, J., Li, Z., Shen, S., and Zhang, F., “Simulation and flight experiments of a quadrotor tail-sitter vertical take-off and landing unmanned aerial vehicle with wide flight envelope,” *International Journal of Micro Air Vehicles*, Vol. 10, No. 4, 2018, pp. 303–317.

[20] Liu, H., Peng, F., Lewis, F. L., and Wan, Y., “Robust tracking control for tail-sitters in flight mode transitions,” *IEEE Transactions on Aerospace and Electronic Systems*, Vol. 55, No. 4, 2018, pp. 2023–2035.

[21] Zhou, J., Lyu, X., Li, Z., Shen, S., and Zhang, F., “A unified control method for quadrotor tail-sitter uavs in all flight modes: Hover, transition, and level flight,” *2017 IEEE/RSJ International Conference on Intelligent Robots and Systems (IROS)*, IEEE, 2017, pp. 4835–4841.

[22] Flores, A., de Oca, A. M., and Flores, G., “A simple controller for the transition maneuver of a tail-sitter drone,” *2018 IEEE Conference on Decision and Control (CDC)*, IEEE, 2018, pp. 4277–4281.

[23] Nascimento, T. P., and Saska, M., “Position and attitude control of multi-rotor aerial vehicles: A survey,” *Annual Reviews in Control*, Vol. 48, 2019, pp. 129–146.

[24] Beard, R. W., and McLain, T. W., *Small unmanned aircraft: Theory and practice*, Princeton university press, 2012.

[25] Lyu, X., Gu, H., Zhou, J., Li, Z., Shen, S., and Zhang, F., “A hierarchical control approach for a quadrotor tail-sitter VTOL UAV and experimental verification,” *2017 IEEE/RSJ International Conference on Intelligent Robots and Systems (IROS)*, IEEE, Vancouver, BC, 2017, pp. 5135–5141.

[26] Johansen, T. A., and Fossen, T. I., “Control allocation—A survey,” *Automatica*, Vol. 49, No. 5, 2013, pp. 1087–1103.

[27] Harkegard, O., “Efficient active set algorithms for solving constrained least squares problems in aircraft control allocation,” *Proceedings of the 41st IEEE Conference on Decision and Control*, 2002., Vol. 2, IEEE, 2002, pp. 1295–1300.

[28] Wang, S., Dai, X., Ke, C., and Quan, Q., “RflySim: A rapid multicopter development platform for education and research based on Pixhawk and MATLAB,” *2021 International Conference on Unmanned Aircraft Systems (ICUAS)*, IEEE, 2021, pp. 1587–1594.

[29] Dai, X., Ke, C., Quan, Q., and Cai, K.-Y., “RFlySim: Automatic test platform for UAV autopilot systems with FPGA-based hardware-in-the-loop simulations,” *Aerospace Science and Technology*, Vol. 114, 2021, p. 106727.

[30] rflysim.com, “rflysim,” <https://rflysim.com/en/index.html>, 2020. Accessed January 1, 2023.

[31] Pucci, D., Hamel, T., Morin, P., and Samson, C., “Nonlinear control of PVTOL vehicles subjected to drag and lift,” *2011 50th IEEE Conference on Decision and Control and European Control Conference*, IEEE, 2011, pp. 6177–6183.